



Article

Co₃O₄ Nanoneedle Array Grown on Carbon Fiber Paper for Air Cathodes towards Flexible and Rechargeable Zn–Air Batteries

Ziyuan Li, Wenjia Han, Peng Jia , Xia Li, Yifei Jiang * and Qijun Ding *

State Key Laboratory of Biobased Material and Green Papermaking, Qilu University of Technology, Shandong Academy of Sciences, Jinan 250353, China; ziyuanli97@126.com (Z.L.); hwj200506@163.com (W.H.); milai19871219@163.com (P.J.); sqlixia126@126.com (X.L.)

* Correspondence: jiangyf@qlu.edu.cn (Y.J.); xianshengding@qlu.edu.cn (Q.D.)

Abstract: An economical and efficient method is developed for preparing flexible cathodes. In this work, a dense mesoporous Co₃O₄ layer was first hydrothermally grown in situ on the surface of chopped carbon fibers (CFs), and then carbon fiber paper (Co₃O₄/CP) was prepared by a wet papermaking process as a flexible zinc-air battery (ZAB). The high-performance air cathode utilizes the high specific surface area of a single chopped carbon fiber, which is conducive to the deposition and adhesion of the Co₃O₄ layer. Through the wet papermaking process, Co₃O₄/CP has ultra-thin, high mechanical stability and excellent electrical conductivity. In addition, the assembled ZAB exhibits relatively excellent electrochemical performance, with a continuous cycle of more than 180 times at a current density of 2 mA·cm⁻². The zinc-air battery can maintain a close fit and work stably and efficiently even under high bending conditions. This process of combining single carbon fibers to prepare ultra-thin, high-density, high-conductivity carbon fiber paper through a papermaking process has huge application potential in the field of flexible wearables.



Citation: Li, Z.; Han, W.; Jia, P.; Li, X.; Jiang, Y.; Ding, Q. Co₃O₄ Nanoneedle Array Grown on Carbon Fiber Paper for Air Cathodes towards Flexible and Rechargeable Zn–Air Batteries. *Nanomaterials* **2021**, *11*, 3321. <https://doi.org/10.3390/nano11123321>

Academic Editor: Lyubov G. Bulusheva

Received: 6 November 2021
Accepted: 6 December 2021
Published: 7 December 2021

Publisher's Note: MDPI stays neutral with regard to jurisdictional claims in published maps and institutional affiliations.



Copyright: © 2021 by the authors. Licensee MDPI, Basel, Switzerland. This article is an open access article distributed under the terms and conditions of the Creative Commons Attribution (CC BY) license (<https://creativecommons.org/licenses/by/4.0/>).

Keywords: flexible zinc-air battery; papermaking; cobalt oxides; carbon fiber; hydrothermal method

1. Introduction

With the improvement of living standards and the development of society, people have higher requirements for environmental protection and convenience of energy utilization [1–3]. At present, secondary energy storage batteries, as a kind of sustainable and recycled clean energy, have been able to replace most of the functions of fossil fuels and are widely used in smart devices, automobiles, aerospace and other fields [4,5]. In recent years, the optimization of secondary energy storage batteries in terms of specific capacity, cycle life, rate performance, etc. has attracted the attention of researchers [6,7]. The emergence of flexible electronic devices such as foldable mobile phones and flexible electronic screens also puts forward high energy density and flexibility requirements for batteries [8–10]. Zinc-air battery (ZAB), as one of the secondary batteries, has excellent performance such as high specific energy and current density, making it an ideal candidate for flexible energy storage equipment [11–13]. However, the current mainstream anode material of ZAB is commercial graphite, which has poor cycle performance and is far below the standard for flexible devices [14,15]. Therefore, there is an urgent need to replace graphite with excellent flexible negative electrode materials.

Carbon fiber (CF), as a flexible inorganic fiber material with a high carbon content, has become the best material to replace commercial graphite electrodes due to its high tensile strength, good electrical conductivity and excellent flexibility [16–18]. Xu et al. assembled a fiber-type zinc-carbon battery using a single carbon fiber as the electrode through a flexible plastic tube to seal the electrolyte [19]. However, the reduction of carbon content and the addition of organic matter inevitably led to the decline of the electrochemical performance of carbon fibers [20]. At present, traditional precious metal catalysts such as Au and Ru are gradually being replaced by non-precious metal catalysts due to the lower cost and

abundant reserves [21]. Charles et al. compared and analyzed the catalytic effects of each element by depositing Ni, Co, Ir oxide and metal compound catalytic layers on the graphene surface [22]. The results show that under the condition of alkaline electrolyte, every non-precious metal system has a certain catalytic effect. Therefore, the performance and chargeability of flexible ZAB largely depends on the dual-function catalyst at the air cathode [23–25]. In addition, as a resource-rich gas, CO₂ has a certain oxidation ability. It can etch micropores on the surface of carbon fibers at high temperatures, increase the specific surface area of carbon fibers, and is an excellent process to improve the surface activity of carbon fibers [26–28].

Among the dual-functional catalysts, nanostructured Co₃O₄ has become one of the most promising catalytic materials due to its nanoporous structure, abundant sources, excellent catalytic activity and alkali resistance [29,30]. Liang et al. grew and synthesized Co₃O₄ nanocrystals on reduced graphene oxide, which proved that carbon-based materials and Co₃O₄ have high oxygen reduction reaction (ORR) activity after hybridization [31]. Bai et al. studied the Co₃O₄ supported structure and proved that the Co₃O₄ layer under the 3D structure has a higher specific surface area and good mesoporous characteristics, and better oxidation ability [32]. However, there are few reports on the application of Co₃O₄ loading in ZAB. Most research focuses on loading directly onto traditional two-dimensional planar structures such as carbon cloth and carbon felt with huge or planar structures. For example, Chen et al. deposited Co(OH)₂ on the surface of carbon cloth by electrophoretic deposition, and prepared a Co₃O₄ catalytic layer by oxidation annealing, which effectively improved the catalytic performance of the air cathode [33]. Zhang et al. prepared a new type of multifunctional catalyst by carbonizing a composite material composed of an imidazole molecular sieve framework and carbon fiber paper, which showed good catalytic activity [34]. It is worth noting that although the two-dimensional structure load achieved a certain catalytic effect, the overall load difficulty is higher than that of the one-dimensional structure. This is due to the decrease in the specific surface area of the carbon fiber due to the oriented multilayer arrangement structure [35,36]. At the same time, high-temperature treatments such as carbonization also require the two-dimensional material itself to have properties such as heat resistance and high bonding strength, and have a high cost. Li et al. developed a bifunctional catalyst composed of atomically layered mesoporous cobalt/nitrogen-doped reduced graphene oxide nanosheets, and prepared a fibrous zinc-air battery, which showed a stable electrochemical performance [37]. Unfortunately, fibrous batteries have the problems of a small size and a low electric capacity [38–40]. Therefore, it is very critical to develop a simple and continuous one-dimensional carbon fiber catalytic layer loading and a two-dimensional integration process.

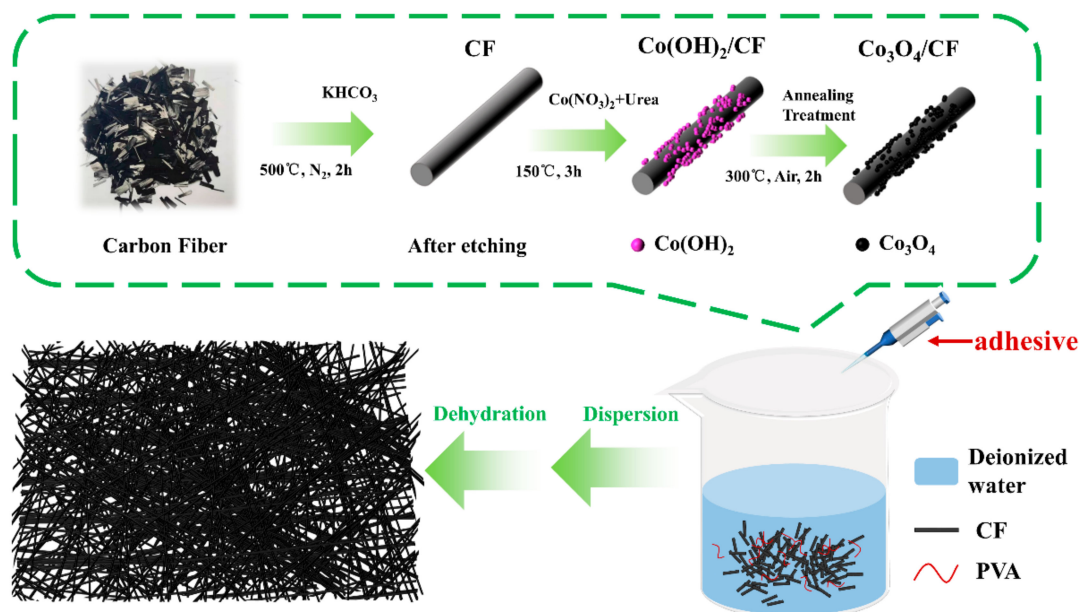
In this work, we used chopped carbon fibers as templates and carbon resources to successfully prepare Co₃O₄/CP air cathodes through hydrothermal reaction synthesis and wet molding processes. ZAB was assembled and prepared by a fast and simple lamination method. The increase in the specific surface area and active sites of the single chopped carbon fiber after the CO₂ etching treatment leads to a greatly increased Co adhesion rate, which is beneficial to improve the electrocatalytic performance. When Co₃O₄/CP was used as the air cathode material, the prepared ZAB exhibited a high round-trip efficiency and a good charge–discharge cycle stability, and it was able to work stably in a variety of folded states. These ultra-thin paper-like composite electrode materials will help to further promote the development of ZAB in the field of various wearable and flexible energy storage, and have great potential.

2. Experimental Section

2.1. Preparation of Air Cathodes for ZAB

All chemicals with analytical grade were purchased from Sigma-Aldrich and were used directly. The air cathode was prepared as the following processes (Scheme 1). Firstly, the carbon fibers (CFs) with the length of 3 mm (Toho Tenax, Tokyo, Japan) were modified via the CO₂ etching at 500 °C for one hour, aiming at removing the impurities, improving

the hydrophilicity and increasing specific surface area (Figure S1). Secondly, $\text{Co}(\text{OH})_2$ nanoneedles were grown on the surface of modified fibers (m-CFs) at $150\text{ }^\circ\text{C}$ for 3 h in a Teflon-lined stainless-steel autoclave containing a hydrothermal solution of 120 mL with 0.02 M $\text{Co}(\text{NO}_3)_2 \cdot 6\text{H}_2\text{O}$ and 0.01 M urea. Thirdly, the $\text{Co}(\text{OH})_2/\text{m-CFs}$ were calcined at $300\text{ }^\circ\text{C}$ for 2 h in a muffle furnace to obtain $\text{Co}_3\text{O}_4/\text{m-CFs}$. Finally, the Co_3O_4 supported on carbon fiber paper ($\text{Co}_3\text{O}_4/\text{CP}$) was produced from CFs by the wet papermaking process. Specifically, the water-based polyurethane was successively used as the dispersant and adhesive agent, and the wet $\text{Co}_3\text{O}_4/\text{CP}$ was pressed at 95 psi and dried at $100\text{ }^\circ\text{C}$. The CP also was prepared according to the above processes for comparison.



Scheme 1. Schematic illustration of the synthetic route to $\text{Co}_3\text{O}_4/\text{CP}$ air cathode.

2.2. Preparation of Hydrogel Electrolyte

The composite hydrogel electrolyte was prepared by a one-pot sol-gel method. Typically, 3.6 g of polyvinyl alcohol (PVA) powder was added to 30 mL of deionized water and stirred at $90\text{ }^\circ\text{C}$ for 12 h to obtain a transparent and viscous PVA solution. Then, the glutaraldehyde (GA, 3.0 wt.% of PVA) and glycerol (GI, 2.0 wt.% of PVA) were added dropwise into the above PVA solution. Subsequently, dilute hydrochloric acid (1.0 wt.%) was added dropwise into the above solution till $\text{pH} = 2$ to promote the cross-linking reaction. Afterwards, the resulting solution was poured into a rectangular mold with a depth of 1 mm and was allowed to stand for 12 h for the sufficient cross-linking to become a hydrogel membrane. Finally, the hydrogel membrane was immersed into 6.0 M KOH for 24 h to obtain a hydrogel electrolyte membrane.

2.3. Fabrication of Flexible Zn-Air Battery

The flexible ZAB was assembled as a 4-layer structure from the below to above: polished and clean copper mesh, air cathode, hydrogel electrolyte membrane and polished and clean zinc foil ($10\text{ mm} \times 30\text{ mm} \times 0.3\text{ mm}$). Importantly, the breathable bandage was used for encapsulation and fixation.

2.4. Characterization

The surface morphologies and elemental mapping analyses of the air cathodes were characterized by a field-emission scanning electron microscope (SEM, Regulus 8220, Hitachi, Japan) equipped with an energy dispersive X-ray spectrometer (EDS, Hitachi, Japan). A high-resolution X-ray micro-computed tomography (Micro-CT, SkyScan 2211, Bruker,

Berlin, Germany) was used to analyze the three-dimensional structures of the air cathode. An X-ray photoelectron spectrometer (XPS, ESCALAB Xi+, Thermo Fisher Scientific, Waltham, MA, USA) was used to analyze the elemental compositions and valences on the surface of air cathodes. The Raman analyses were performed on a laser confocal microscopy Raman spectrometer (Renishaw inVia, Gloucestershire, UK) with 532 nm laser excitation. The phase compositions were ascertained by using an X-ray diffractometer instrument (XRD, D8-ADVANCE, Bruker, Germany). The thermogravimetric (TG) analysis was carried out on a simultaneous thermal analyzer (STA449, Selb, Germany). The mechanical properties of commercial carbon paper (CP), CP and $\text{Co}_3\text{O}_4/\text{CP}$ were tested at room temperature on a texture analyzer (TA. XT plusC, SMS, Surrey, UK). The prepared $\text{Co}_3\text{O}_4/\text{CP}$ was subjected to multiple tensile tests and compared with commercial CP. The Young's modulus is obtained by calculating the slope of the fitted straight line (fitted 5 times respectively, and the results are averaged) [41]. The air cathode was tested by using the four-point probe method.

An electrochemical workstation (CHI660E, Shanghai Chenghua Instrument Co., LTD., Shanghai, China) with a PINE rotating disk electrode (RDE) system was used to test the ORR activity of the $\text{Co}_3\text{O}_4/\text{CP}$ material. Firstly, each air electrode material was ground into powder separately. Then, 4.0 mg of carbon powder material was ultrasonically dispersed in 2 mL of Nafion (5%), absolute ethanol, and deionized water ($v:v:v = 1:1:4$) solution. Then, 20 μL uniform ink was taken and loaded on to the glassy carbon (GC) electrode. Using platinum as the counter electrode and silver chloride as the reference electrode, the cyclic voltammetry scan test (CV) and the linear voltammetry scan test (LSV) were performed at a scan rate of $10 \text{ mV}\cdot\text{s}^{-1}$, and the voltage range is $-1\sim 0.2 \text{ V}$. The RDE test is measured in a 0.1 M KOH solution at room temperature under O_2 saturation at different speeds ranging from 400 to 2025 rpm, and the scan rate is $10 \text{ mV}\cdot\text{s}^{-1}$. The battery charging and discharging polarization test was carried out by the line scan method, and the voltage range is $0\sim 3 \text{ V}$. The number of electrons transferred per oxygen molecule at different potentials during the oxygen reduction reaction (ORR) (n) is calculated according to the Koutecky–Levich (K-L) equation [42]. The OER polarization curve test was carried out in 1.0 M KOH at room temperature, and the scan rate was $10 \text{ mV}\cdot\text{s}^{-1}$. The data representing OER activity were corrected for iR compensation.

The electrochemical properties of ZAB batteries were characterized on the Land battery test system (LAND CT2001A, Wuhan LAND Electronic Co., Ltd., Wuhan, China) by the polarization and galvanostatic charge/discharge test (GCD). Check the ZAB rate stability by changing the discharge current density to 0.05, 0.1, 0.5, 1, 2, 5, $1 \text{ mA}\cdot\text{cm}^{-2}$, and the discharge time is 10 min. The GCD test is carried out at a current density of $2 \text{ mA}\cdot\text{cm}^{-2}$, the charging and discharging time is 10 min each, and the protection voltage is set to $0.5\sim 2.5 \text{ V}$.

3. Results and Discussion

As shown in Figure S2, after CO_2 etching treatment, the hydrophilicity of the carbon fiber is significantly improved. Therefore, the EDS results show that the fiber surface is uniformly loaded with Co, O, and C elements (Figure S3). After annealing, $\text{Co}_3\text{O}_4/\text{CF}$ maintained the high adhesion of the catalytic layer (Figure 1a). The EDS element mapping image also showed that Co (yellow), O (red) and C (blue) coexist and were evenly distributed on the carbon fiber's surface. The growth area and density of the Co element were relatively high, and the nanosheet layered structure can be clearly observed on the surface of the carbon fiber, and had a high signal intensity of Co (Table S1). After wet papermaking processes such as dispersion and suction filtration, an air cathode $\text{Co}_3\text{O}_4/\text{CP}$ was obtained. The loading of the Co element remains high and uniform, and the Co_3O_4 catalytic layer showed a stable adhesion performance (Figure 1b).

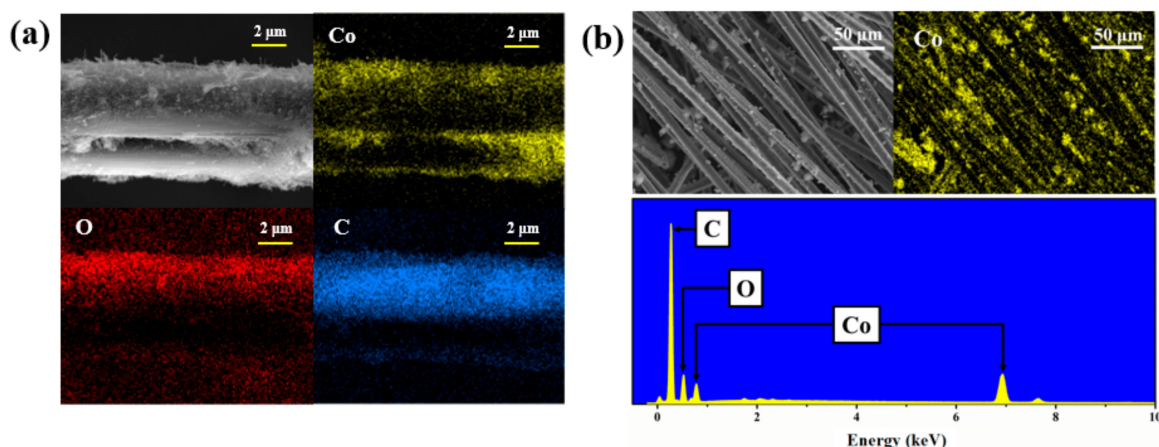


Figure 1. (a) EDS image of $\text{Co}_3\text{O}_4/\text{CF}$ surface, (b) SEM and Co element distribution image of $\text{Co}_3\text{O}_4/\text{CP}$.

Figure 2 shows the Micro-CT image of $\text{Co}_3\text{O}_4/\text{CP}$. The $\text{Co}_3\text{O}_4/\text{CF}$ after hydrothermal growth and annealing presented a disorderly interlaced stacking state (Figure 2a,c). This multi-layer staggered structure enables a single carbon fiber to contact and bond efficiently in a three-dimensional space, which is beneficial to improve electrical conductivity. A small amount of resin adhesive was uniformly distributed in the form of small particles at the fiber interweaving points, ensuring the mechanical strength of $\text{Co}_3\text{O}_4/\text{CP}$ without flocculation (Figure 2b). The highly loose pore structure of $\text{Co}_3\text{O}_4/\text{CP}$ improved the electrochemical performance of flexible zinc-air battery such as rate, constant current charge and discharge.

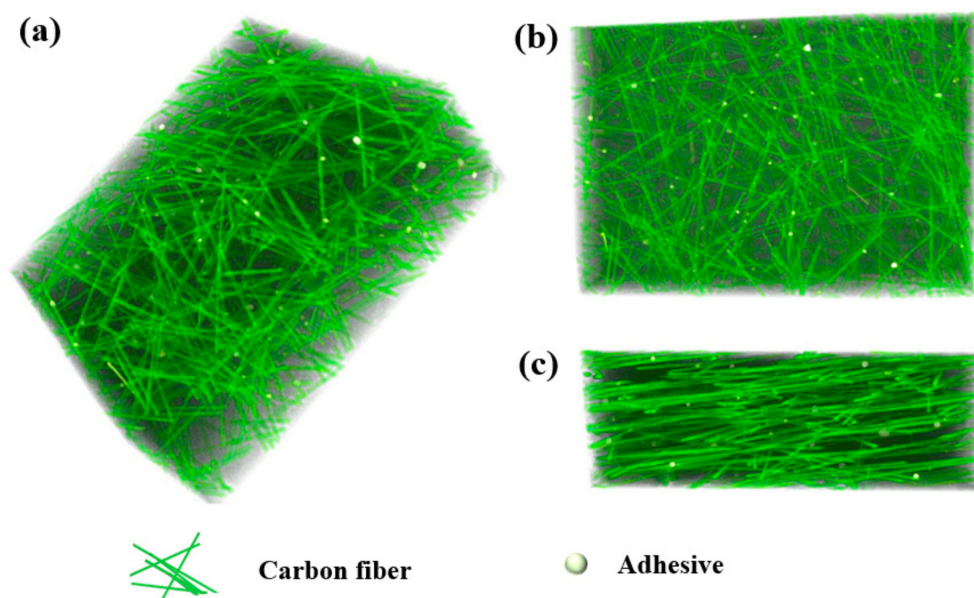


Figure 2. Micro-CT image of $\text{Co}_3\text{O}_4/\text{CP}$ air cathode. (a) Front view, (b) Top view, (c) Side view.

In order to further prove the loading of the Co_3O_4 layer on the surface of the carbon fiber, X-ray photoelectron spectroscopy (XPS) tests were performed on the CF, $\text{Co}(\text{OH})_2/\text{CF}$, and $\text{Co}_3\text{O}_4/\text{CF}$ in the process to observe their chemical composition and valence, as shown in Figure 3. The XPS spectra in Figure 3a,c show that the prepared $\text{Co}(\text{OH})_2/\text{CF}$ and $\text{Co}_3\text{O}_4/\text{CF}$ both contain Co, O and C elements, which are consistent with the EDS results. The C element comes from chopped carbon fiber, the XPS image of the original m-CF in Figure S4 also proves this. Figure 3b shows the XPS spectrum curve of Co 2p in $\text{Co}(\text{OH})_2/\text{CF}$. The curve showed two main peaks at 796.5 and 780.2 eV, which correspond to the Co 2p_{1/2} and Co 2p_{3/2} orbitals of the metal ion Co. By peak fitting, the Co 2p_{3/2}

peak in Figure 3d could be divided into two peaks, at 795.3 and 780.2 eV, indicating that the Co^{2+} and Co^{3+} states coexist in the $\text{Co}_3\text{O}_4/\text{CF}$ sample. In addition, the binding energy difference (spin-orbit splitting) between the $\text{Co } 2p_{3/2}$ and $\text{Co } 2p_{1/2}$ peaks was 15.2 eV, which is also very consistent with the binding energy difference of pure Co_3O_4 reported in the literature [33].

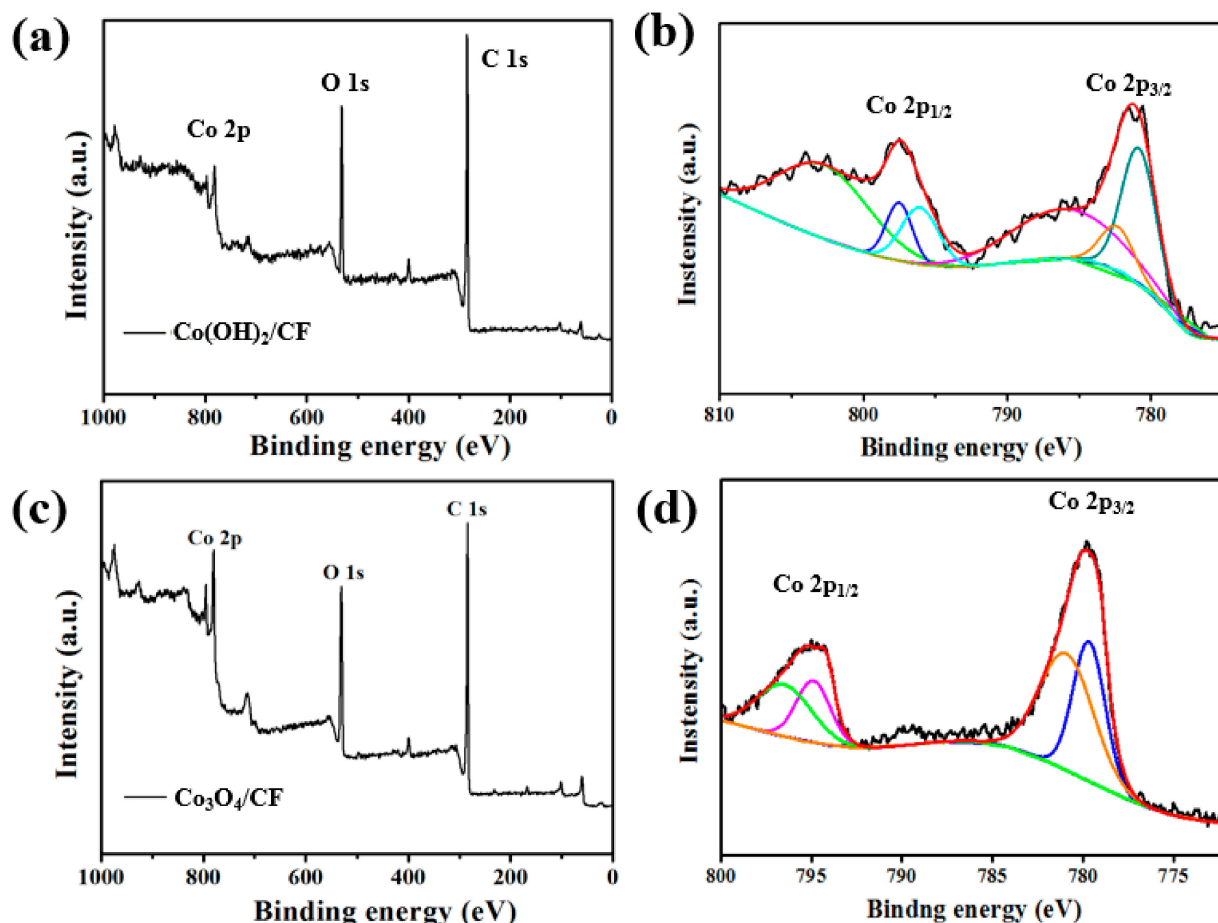


Figure 3. (a) XPS survey spectrum, (b) Co 2p of an $\text{Co}(\text{OH})_2/\text{CF}$, and (c) XPS survey spectrum, (d) Co 2p of an $\text{Co}_3\text{O}_4/\text{CF}$.

As shown in Figure 4a, CF, $\text{Co}(\text{OH})_2/\text{CF}$ and $\text{Co}_3\text{O}_4/\text{CF}$ all exhibited two characteristic Raman peaks of carbon at 1350 cm^{-1} and 1596 cm^{-1} . It corresponds to disordered carbon and sp^2 carbon atom E_{2g} mode scattering, respectively. In addition, for $\text{Co}_3\text{O}_4/\text{CP}$ and $\text{Co}_3\text{O}_4/\text{CF}$, the Raman spectrum clearly shows obvious peaks at 668 cm^{-1} , and new peaks are also generated at 465 and 510 cm^{-1} . These peaks are characteristic of Co_3O_4 [16,33,37]. The above results further proved that Co_3O_4 was successfully loaded on the surface of carbon fiber. By comparing the peak intensity of $\text{Co}_3\text{O}_4/\text{CF}$ and $\text{Co}_3\text{O}_4/\text{CP}$, it is proved that $\text{Co}_3\text{O}_4/\text{CP}$ still maintains a high catalytic layer loading. XRD measurements were performed on each sample, and the CF can only observe an obvious diffraction peak at the 2θ value of 25.4 (Figure 4b). The difference is that $\text{Co}_3\text{O}_4/\text{CP}$ and $\text{Co}_3\text{O}_4/\text{CF}$ have new diffraction peaks observed at 38.2 , 45.4 , 59.8 , and 66.2 , which proves the formation of the Co_3O_4 layer. This is also consistent with the above description. Since the formed Co_3O_4 supporting layer is thinner than the main body of carbon fiber, the XRD curve is still dominated by carbon fiber.

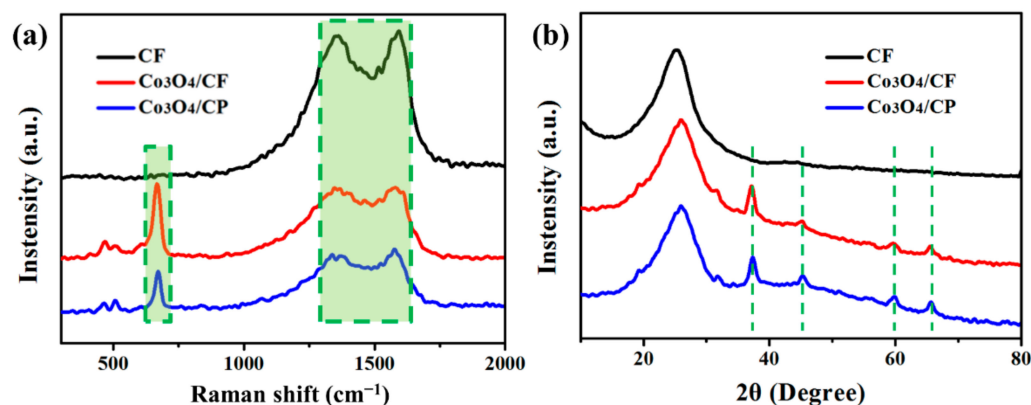


Figure 4. (a) Raman spectra of CF, $\text{Co}_3\text{O}_4/\text{CF}$, $\text{Co}_3\text{O}_4/\text{CP}$; (b) XRD spectra of CF, $\text{Co}_3\text{O}_4/\text{CF}$, $\text{Co}_3\text{O}_4/\text{CP}$.

Due to the use of wet forming, hot pressing and drying, the structure of CP and $\text{Co}_3\text{O}_4/\text{CP}$ is closer, the internal resistance is reduced (Figure S5), and the conductivity is improved. Figure S6 shows and compares the cyclic voltammetry (CV) characteristic curve and the linear sweep voltammetry (LSV) curve of the air cathode before and after the Co_3O_4 load. From the CV curve, the electrode loaded with Co_3O_4 has significantly improved redox onset potential and peak current density than the unloaded electrode. The results show that the electrochemical performance of the oxidation-reduction reaction of Co_3O_4 supported by CP has been improved. Figure S7 shows the OER curve measured by using commercial CP and $\text{Co}_3\text{O}_4/\text{CP}$ electrode in 1.0 M KOH solution. Under the same current density, $\text{Co}_3\text{O}_4/\text{CP}$ is significantly higher than commercial CP, showing certain OER activity. In addition, $\text{Co}_3\text{O}_4/\text{CP}$ has a relatively low OER Tafel slope, indicating a favorable kinetic OER process. In order to show the ORR kinetics of the prepared air cathode, the ORR LSV of the $\text{Co}_3\text{O}_4/\text{CP}$ electrode was measured at a different scan rate (Figure S8). According to the KL formula, the number of transferred electrons from -0.40 to -0.60 V to RHE is about 3.3 (Figure S8 insert), which is relatively close to the current number of commercial catalytic transfer electrons, showing a certain catalytic performance [43]. This indicates the four-electron ORR mechanism of the $\text{Co}_3\text{O}_4/\text{CP}$ sample.

As shown in Figure 5a, the $\text{Co}_3\text{O}_4/\text{CP}$ electrode exhibits excellent bendability and flexibility. Figure 5b displays TG curves of the CF, $\text{Co}_3\text{O}_4/\text{CP}$ and the commercial CP. All the curves show two evident weight losses. The first occurred at 200 °C, which means that the binder starts to decompose. The rapid weight loss at around 420 °C is mainly due to the complete pyrolysis of the binder waterborne polyurethane adhesive and the pyrolysis inside the carbon fiber. According to the TG curve comparison between CP and $\text{Co}_3\text{O}_4/\text{CP}$ samples, the loading of Co_3O_4 accounts for 1.5% of the total carbon fiber mass. In addition, by comparing with commercial CP, carbon fiber paper prepared by papermaking method maintains a higher heat resistance while using less adhesive. The tensile stress–strain curves of $\text{Co}_3\text{O}_4/\text{CP}$ and commercial CP are shown in Figure 5c. The $\text{Co}_3\text{O}_4/\text{CP}$ have a significant improvement effect in stress intensity and tensile deformation properties compared to commercial CP. $\text{Co}_3\text{O}_4/\text{CP}$ can reach a maximum stress of 42.5 MPa and a strain of 2.25%. By comparing $\text{Co}_3\text{O}_4/\text{CP}$ with CP, it was found that the loading of the catalytic layer Co_3O_4 had no obvious influence on the strength and tensile deformation, mainly because the supporting layer was thin. In addition, the average Young's modulus of $\text{Co}_3\text{O}_4/\text{CP}$ is 22.9 MPa, which is not significant compared to the 19.4 MPa of commercial CP (Figure S9). This indicates that the loading of Co_3O_4 and the calcination process have little effect on the stiffness of carbon fiber paper, and $\text{Co}_3\text{O}_4/\text{CP}$ can retain the original flexibility.

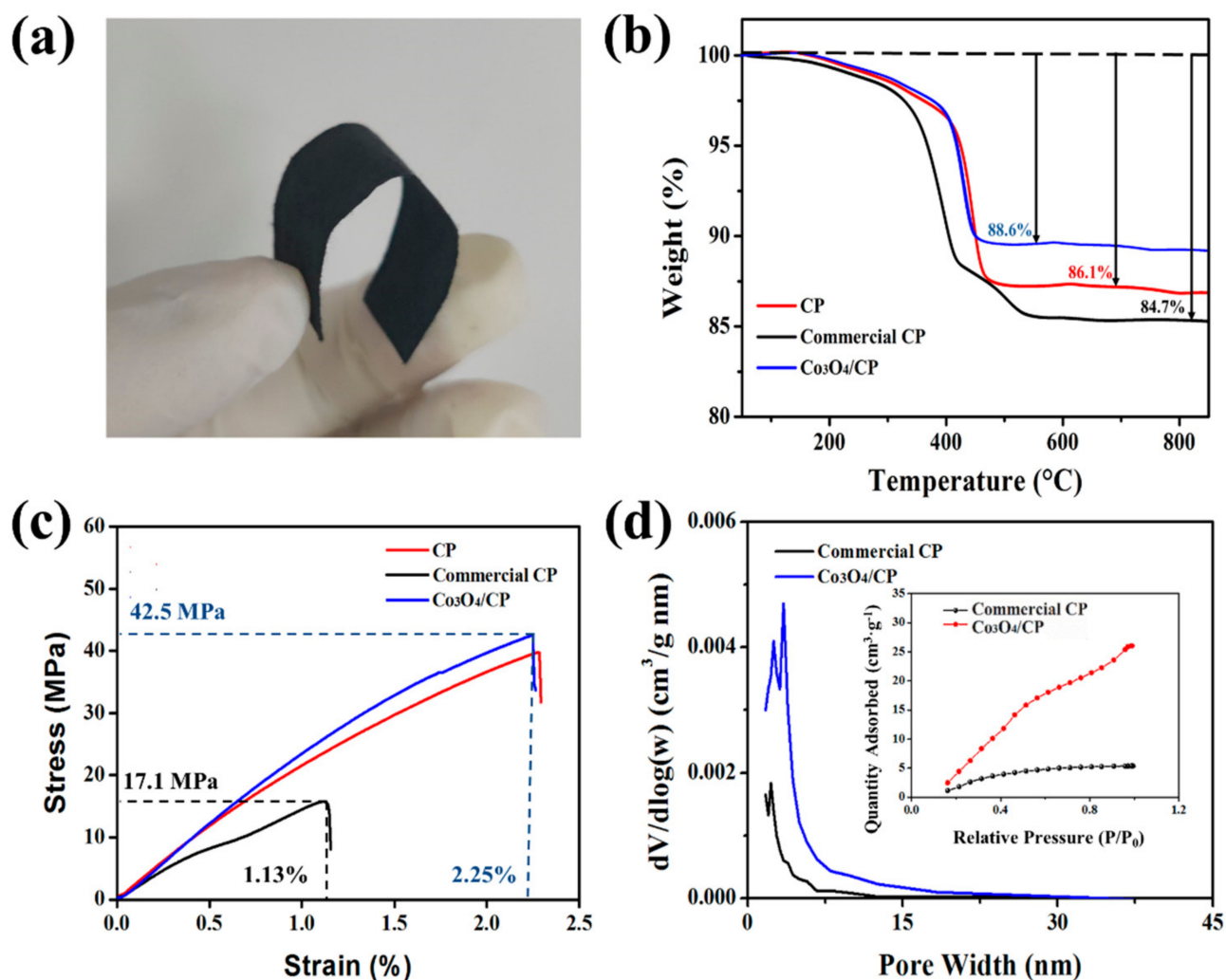


Figure 5. (a) Schematic photo of Co₃O₄/CP; (b) TGA spectra of CP, Co₃O₄/CP, Co₃O₄/CP; (c) Tensile performance test of CP, commercial CP, Co₃O₄/CP; (d) Nitrogen desorption curve.

The improvement of the mechanical properties of the Co₃O₄/CP material were attributed to the increase in the interwoven structure of the chopped carbon fibers and the point bonding effect of the adhesive. Co₃O₄/CP exhibits a higher mesoporous content structure, with a mesoporous diameter between 2 and 5 nm (Figure 5d). The porous structure of Co₃O₄/CP can buffer the volume change of the electrode during charge and discharge, which is a benefit for improving the electrochemical performance of the electrode [8].

Based on the excellent flexibility and high-efficiency catalytic performance of the Co₃O₄/CP electrode, a flexible rechargeable zinc-air battery was prepared. The open circuit potential (OCP) of the flexible ZAB with a Co₃O₄/CP electrode measured by the electrochemical workstation can reach 1.34 V (as shown in Figure 6a), which is consistent with the value reported in the literature for the zinc-air battery. Figure 6b shows the charging and discharging electric polarization curve of the flexible ZAB. Compared with ZAB using commercial CP as the air cathode, ZAB using Co₃O₄/CP air cathode exhibits a lower overpotential during charging and discharging. The gap becomes more obvious with the increase in current density.

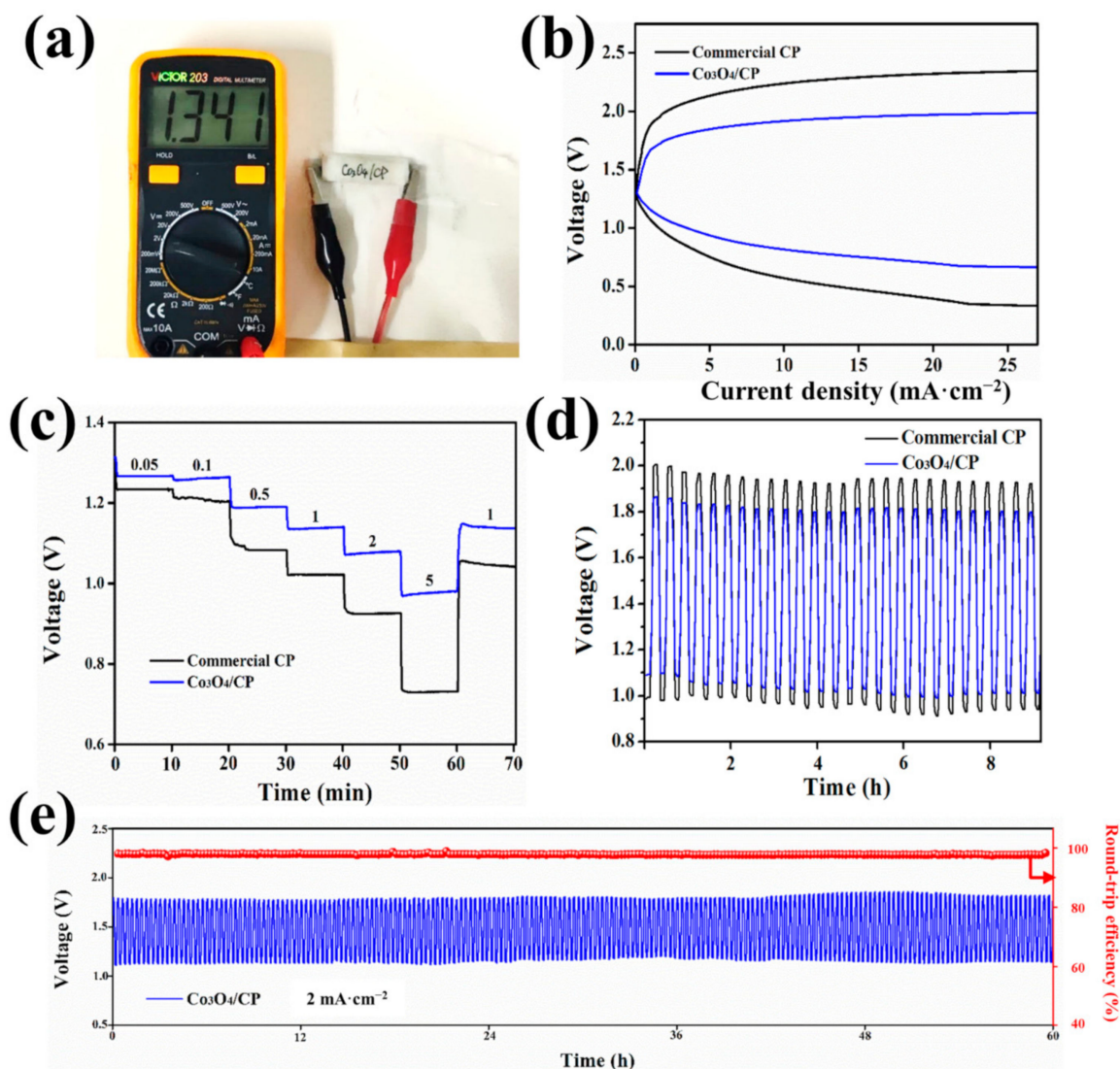


Figure 6. (a) Open circuit voltage of $\text{Co}_3\text{O}_4/\text{CP-ZAB}$; (b) Comparison of ZAB charge and discharge polarization curves under different electrodes; (c) Voltage performance under different discharge currents; (d) Comparison of constant current charge and discharge curves of 2 mA cm^{-2} ; (e) Constant current cycle charge-discharge curve of $\text{Co}_3\text{O}_4/\text{CP-ZAB}$ at a current density of 2 mA cm^{-2} .

Figure 6c show the discharge performance of different flexible zinc-air batteries under varying current density conditions. With the increase of the discharge current density, the discharge voltage of ZAB decreased significantly. Compared with commercial CP-ZAB, $\text{Co}_3\text{O}_4/\text{CP-ZAB}$ has a higher discharge voltage at the same current density. This difference was more pronounced at high current densities. The reasons for the excellent electrocatalytic performance of $\text{Co}_3\text{O}_4/\text{CP-ZAB}$ are as follows: the tight nanostructure load between the Co_3O_4 layer and the surface of the carbon fiber and the abundant mesoporous structure provide a channel for the rapid transmission of electrons during the catalytic reaction; the close combination of carbon fiber active material and gel electrolyte; the tight three-dimensional interweaving structure of carbon fiber improves its electrical conductivity. In order to further study the stability of $\text{Co}_3\text{O}_4/\text{CP}$ electrodes during cycling, ZAB was tested with constant current charge and discharge. As shown in Figure 6d, compared to commercial CP, $\text{Co}_3\text{O}_4/\text{CP}$ ZAB exhibits a lower charge and discharge overpotential, which means that the battery is more rechargeable. In addition, at a current density of $2 \text{ mA}\cdot\text{cm}^{-2}$, commercial CP ZAB cycle time is less than 36 h, and the cycle number is about 100 times (Figure S10). The $\text{Co}_3\text{O}_4/\text{CP}$ air cathode ZAB can continuously cycle and stably

charge and discharge for more than 60 h, and the number of cycles can reach more than 180 times. Compared with other carbon fiber substrate cathode research in recent years, the $\text{Co}_3\text{O}_4/\text{CP}$ flexible ZAB still shows good stability (as shown in Table S2).

The flexible zinc-air battery was subjected to long-term charge–discharge cycle tests under bending angles of 0° , 60° , and 180° . As shown in Figure 7a, the results proved that ZAB assembled with $\text{Co}_3\text{O}_4/\text{CP}$ as the base still had a relatively consistent long-term work in a highly bending working environment. Life, and the voltage range, can also be stabilized at 1.0~2.0 V. This proves that the laminated zinc-air battery has a relatively excellent flexible working performance. It can be seen from Figure 7b that, at any given bending angle, the manufactured ZAB has excellent stability without significant changes in potential. In addition, at a current of $2\text{ mA}\cdot\text{cm}^{-2}$, the highly curved flexible ZAB can still be discharged stably for 33.7 h, with a discharge capacity of $67.4\text{ mAh}\cdot\text{cm}^{-2}$. This demonstrates the excellent energy conversion performance of the $\text{Co}_3\text{O}_4/\text{CP}$ flexible ZAB.

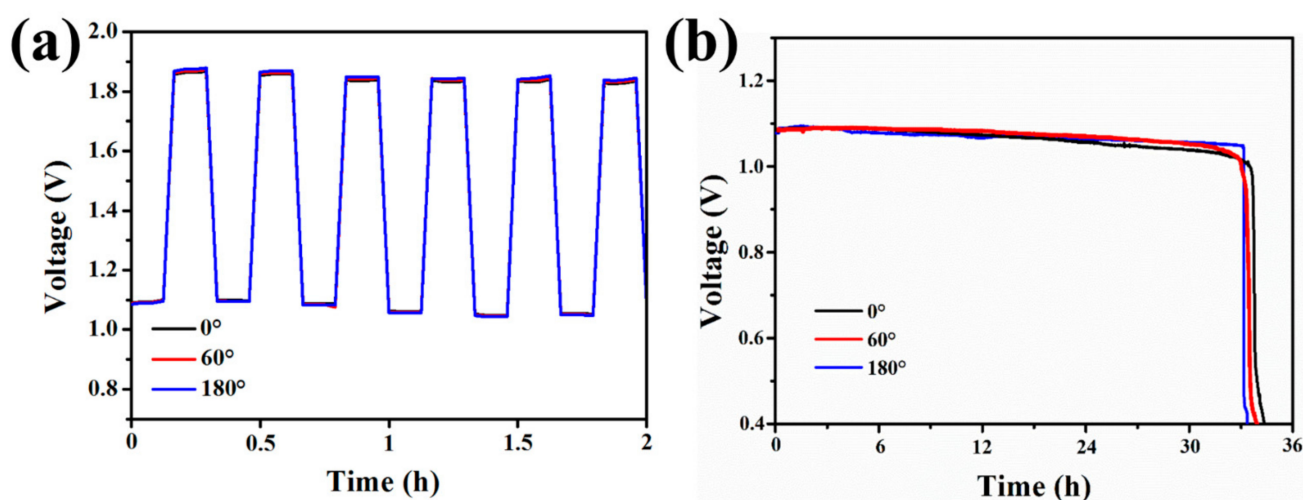


Figure 7. The flexible performance of ZAB battery. (a) Constant current charging and discharging cycles under different bending angles of the battery. (b) Battery discharge voltage performance under different bending angles.

According to the $\text{Co}_3\text{O}_4/\text{CP}$ -ZAB preparation and assembly process described above, three ZABs encapsulated by breathable gauze and aluminum plastic film are connected in series. As shown in Figure 8a, the three ZAB groups exhibited a relatively high 4.12V open circuit voltage. Wearing it as a flexible device on the hand, its output voltage basically remains unchanged (Figure 8b). In addition, these ZABs can be used to charge light-emitting diode (LED) screens through a serial bus transmission interface (Figure 8c). This proves that it has good wearable energy storage device performance.

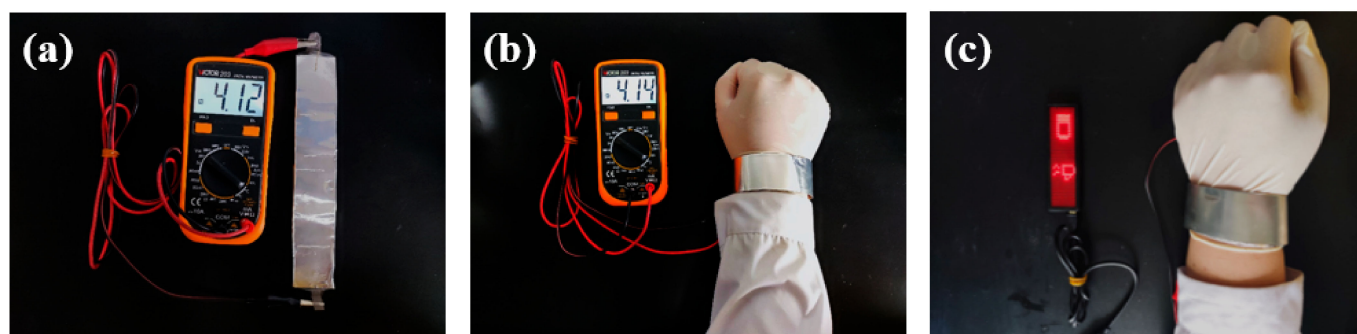


Figure 8. Flexible zinc-air battery assembly array and its application. (a) Array static voltage; (b) array flexibility; (c) array wear voltage.

4. Conclusions

In summary, an economical and efficient method is developed for preparing flexible cathodes. In this work, a dense mesoporous Co_3O_4 layer was first hydrothermally grown in situ on the surface of a single chopped carbon fiber (CF), and then carbon fiber paper ($\text{Co}_3\text{O}_4/\text{CP}$) was prepared by a wet papermaking process as a flexible zinc-air battery. Thanks to the high catalytic performance of the Co_3O_4 layer and the high conductivity of the active material, the quality activity of the $\text{Co}_3\text{O}_4/\text{CP}$ electrode for oxygen reduction and precipitation reactions is far higher than that of commercial carbon paper of the same quality. Through the wet papermaking process, $\text{Co}_3\text{O}_4/\text{CP}$ has a high mechanical stability and excellent electrical conductivity. In addition, the assembled zinc-air battery exhibits excellent electrochemical performance, with a continuous cycle of more than 180 times at a current density of $2\text{mA}\cdot\text{cm}^{-2}$. This traditional papermaking method provided a new pathway for designing flexible air-cathodes. Combining the uniform loading of the Co_3O_4 catalytic layer with the carbon fiber network integration process improves the uniformity of internal loading and improves process continuity. Consequently, this paper-based air cathode would hold considerable potential for rechargeable flexible ZAB applications.

Supplementary Materials: The following are available online at <https://www.mdpi.com/article/10.3390/nano11123321/s1>, Figure S1. SEM images (a) CF, (b) m-CF. Figure S2. Contact angle image of (a) commercial CP, (b) CP and (c) $\text{Co}_3\text{O}_4/\text{CP}$. Figure S3 (a) SEM image of $\text{Co}(\text{OH})_2/\text{m-CF}$ and the corresponding EDS elemental mapping images of (b) Co, (c) O and (d) C. Figure S4. Survey XPS spectrum of m-CFs. Figure S5. (a) various cathode conductivity data graphs; and actual detection images of (b) commercial CP, (c) CP, (d) $\text{Co}_3\text{O}_4/\text{CP}$. Figure S6. ORR performances of the commercial CP and $\text{Co}_3\text{O}_4/\text{CP}$: (a) CV curves; (b) LSV curves. Figure S7. OER performances of the commercial CP and $\text{Co}_3\text{O}_4/\text{CP}$. Figure S8 ORR polarization curves of $\text{Co}_3\text{O}_4/\text{CFP}$ at different rotation speeds in O_2 -saturated 0.1 M KOH solution. Figure S9. Repeated tensile test data of (a) commercial CP, (b) $\text{Co}_3\text{O}_4/\text{CP}$. Figure S10. GCD cycle curves of the flexible zinc-air battery assembled with commercial CP. Table S1. The weight percentage of elements in $\text{Co}_3\text{O}_4/\text{CP}$ air cathode. Table S2. A summary of the battery performance of ZAB based on carbon fiber-based air electrodes in the literature. References [44,45] were cited in Supplementary Materials.

Author Contributions: Conceptualization, Z.L. and P.J.; methodology, P.J.; software, Q.D.; validation, Z.L., Y.J. and Q.D.; formal analysis, Y.J.; investigation, Z.L.; resources, W.H.; data curation, Z.L.; writing—original draft preparation, Z.L.; writing—review and editing, Z.L.; visualization, X.L.; supervision, Y.J.; project administration, W.H.; funding acquisition, Y.J. All authors have read and agreed to the published version of the manuscript.

Funding: This research was funded by the National Key Research Program of China (No. 2020YFC1910301); Innovation Pilot Project of Integration of Science, Education and Industry of Shandong Province (No. 2020KJC-ZD06); the Foundation of State Key Laboratory of Biobased Material and Green Papermaking, Qilu University of Technology, Shandong Academy of Sciences (Nos. ZZ20200107, ZZ20200118, ZZ20190111 and ZZ20210111); National Natural Science Foundation of China (No. 22001140); Natural Science Foundation of Shandong Province, China (No. ZR20200B002).

Data Availability Statement: The data presented in this study are available on reasonable request from the corresponding author.

Conflicts of Interest: The authors declare no conflict of interest.

References

1. Fu, J.; Zhang, J.; Song, X.; Zarrin, H.; Tian, X.; Qiao, J.; Rasen, L.; Li, K.; Chen, Z. A flexible solid-state electrolyte for wide-scale integration of rechargeable zinc–air batteries. *Energy Environ. Sci.* **2015**, *9*, 663–670. [[CrossRef](#)]
2. Park, J.; Park, M.; Nam, G.; Lee, J.-S.; Cho, J. All-solid-state cable-type flexible zinc-air battery. *Adv. Mater.* **2015**, *27*, 1396–1401. [[CrossRef](#)] [[PubMed](#)]
3. Fan, X.; Liu, J.; Song, Z.; Han, X.; Deng, Y.; Zhong, C.; Hu, W. Porous nanocomposite gel polymer electrolyte with high ionic conductivity and superior electrolyte retention capability for long-cycle-life flexible zinc–air batteries. *Nano Energy* **2019**, *56*, 454–462. [[CrossRef](#)]
4. Zhu, M.; Wu, J.; Wang, Y.; Song, M.; Long, L.; Siyal, S.H.; Yang, X.; Sui, G. Recent advances in gel polymer electrolyte for high-performance lithium batteries. *J. Energy Chem.* **2019**, *37*, 126–142. [[CrossRef](#)]

5. He, R.; Liang, H.; Li, C.; Bai, J. Enhanced photocatalytic hydrogen production over $\text{Co}_3\text{O}_4@g\text{-C}_3\text{N}_4$ p-n junction adhering on one-dimensional carbon fiber. *Colloids Surf. A Physicochem. Eng. Asp.* **2020**, *586*, 124200. [[CrossRef](#)]
6. Sheng, J.; Tong, S.; He, Z.; Yang, R. Recent developments of cellulose materials for lithium-ion battery separators. *Cellulose* **2017**, *24*, 4103–4122. [[CrossRef](#)]
7. Manuel, S.A. Review on gel polymer electrolytes for lithium batteries. *Eur. Polym. J.* **2006**, *42*, 21–42. [[CrossRef](#)]
8. Wang, W.; Liu, Y.; Wang, M.; Ren, G.; Wu, S.; Shen, J. Facilely prepared oxidized carbon Fiber@ Co_3O_4 @ RGO as negative electrode for a novel asymmetric supercapacitor with high areal energy and power density. *Appl. Surf. Sci.* **2018**, *450*, 66–76. [[CrossRef](#)]
9. Yang, H.; Leow, W.R.; Chen, X. 3D printing of flexible electronic devices. *Small Methods* **2018**, *450*, 1700259. [[CrossRef](#)]
10. Gong, M.; Zhang, L.; Wan, P. Polymer nanocomposite meshes for flexible electronic devices. *Prog. Polym. Sci.* **2020**, *107*, 101279. [[CrossRef](#)]
11. Pan, Z.; Yang, J.; Zang, W.; Kou, Z.; Wang, C.; Ding, X.; Guan, C.; Xiong, T.; Chen, H.; Zhang, Q.; et al. All-solid-state sponge-like squeezable zinc-air battery. *Energy Storage Mater.* **2019**, *23*, 375–382. [[CrossRef](#)]
12. Mainar, A.R.; Iruin, E.; Blázquez, J.A. High performance secondary zinc-air/silver hybrid battery. *J. Energy Storage* **2021**, *33*, 102103. [[CrossRef](#)]
13. Li, Y.; Dai, H. Recent advances in zinc-air batteries. *Chem. Soc. Rev.* **2014**, *43*, 5257–5275. [[CrossRef](#)] [[PubMed](#)]
14. Li, Y.; Gong, M.; Liang, Y.; Feng, J.; Kim, J.-E.; Wang, H.; Hong, G.; Zhang, B.; Dai, H. Advanced zinc-air batteries based on high-performance hybrid electrocatalysts. *Nat. Commun.* **2013**, *4*, 1805. [[CrossRef](#)] [[PubMed](#)]
15. Zhong, Y.; Pan, Z.; Wang, X.; Yang, J.; Qiu, Y.; Xu, S.; Lu, Y.; Huang, Q.; Li, W. Hierarchical Co_3O_4 Nano-micro arrays featuring superior activity as cathode in a flexible and rechargeable zinc-air battery. *Adv. Sci.* **2019**, *6*, 1802243. [[CrossRef](#)] [[PubMed](#)]
16. Wang, Z.; Zhang, X.; Sun, Y.; Zhang, H.; Wang, C.; Xie, A. Facile synthesis and electrochemical performance of nitrogen-doped porous hollow coaxial carbon fiber/ Co_3O_4 composite. *Ceram. Int.* **2018**, *44*, 5848–5854. [[CrossRef](#)]
17. Yang, S.; Cheng, Y.; Xiao, X.; Pang, H. Development and application of carbon fiber in batteries—Science Direct. *Chem. Eng. J.* **2020**, *384*, 123294. [[CrossRef](#)]
18. Wang, Z.; Ang, J.; Liu, J.; Ma, X.Y.D.; Kong, J.; Zhang, Y.; Yan, T.; Lu, X. FeNi alloys encapsulated in N-doped CNTs-tangled porous carbon fibers as highly efficient and durable bifunctional oxygen electrocatalyst for rechargeable zinc-air battery. *Appl. Catal. B Environ.* **2019**, *263*, 118344. [[CrossRef](#)]
19. Xu, N.; Zhang, Y.; Wang, M.; Fan, X.; Zhang, T.; Peng, L.; Zhou, X.-D.; Qiao, J. High-performing rechargeable/flexible zinc-air batteries by coordinated hierarchical Bi-metallic electrocatalyst and heterostructure anion exchange membrane. *Nano Energy* **2019**, *65*, 104021. [[CrossRef](#)]
20. Wang, H.-F.; Tang, C.; Wang, B.; Li, B.-Q.; Cui, X.; Zhang, Q. Defect-rich carbon fiber electrocatalysts with porous graphene skin for flexible solid-state zinc-air batteries. *Energy Storage Mater.* **2018**, *15*, 124–130. [[CrossRef](#)]
21. Cheng, W.; Lu, X.F.; Luan, D.; Lou, X.W. NiMn-based bimetal-organic framework nanosheets supported on multi-channel carbon fibers for efficient oxygen electrocatalysis. *Angew. Chem. Int. Ed.* **2020**, *59*, 18234–18239. [[CrossRef](#)] [[PubMed](#)]
22. McCrory, C.C.L.; Jung, S.; Peters, J.C.; Jaramillo, T.F. Benchmarking heterogeneous electrocatalysts for the oxygen evolution reaction. *J. Am. Chem. Soc.* **2013**, *135*, 16977–16987. [[CrossRef](#)] [[PubMed](#)]
23. Fan, W.; Yuan, H.; Huang, J. A bio-inspired nanofibrous $\text{Co}_3\text{O}_4/\text{TiO}_2$ /carbon composite as high-performance anodic material for lithium-ion batteries. *J. Alloys Compd.* **2020**, *819*, 153375.
24. Yin, J.; Li, Z.; Yu, Y.; Lv, Y.; Song, K.; Yang, B.; Yuan, L.; Hu, X. Facile electrodeposition of MFe_2O_4 (M = Co, Fe) on carbon cloth as air cathodes for Li-O₂ batteries. *Ceram. Int.* **2019**, *45*, 13401–13408. [[CrossRef](#)]
25. Guan, Q.; Li, Y.; Bi, X.; Yang, J.; Zhou, J.; Li, X.; Cheng, J.; Wang, Z.; Wang, B.; Lu, J. Dendrite-free flexible fiber-shaped Zn battery with long cycle life in water and air. *Adv. Energy Mater.* **2019**, *9*, 1901434. [[CrossRef](#)]
26. Lee, J.H.; Lee, S.H.; Suh, D.H. High micropore number and specific surface of carbon fibers pretreated with a swarm of CO_2 micro-nanobubbles. *Environ. Chem. Lett.* **2021**, *19*, 3565–3571. [[CrossRef](#)]
27. Choma, J.; Osuchowski, L.; Marszewski, M.; Dziura, A.; Jaroniec, M. Developing microporosity in Kevlar[®]-derived carbon fibers by CO_2 activation for CO_2 adsorption. *J. CO₂ Util.* **2016**, *16*, 17–22. [[CrossRef](#)]
28. Zhang, J.; Jia, K.; Lin, L.; Zhao, W.; Quang, H.T.; Sun, L.; Li, T.; Li, Z.; Liu, X.; Zheng, L.; et al. Large-area synthesis of superclean graphene via selective etching of amorphous carbon with carbon dioxide. *Angew. Chem. Int. Ed.* **2019**, *58*, 14446–14451. [[CrossRef](#)] [[PubMed](#)]
29. Ji, D.; Fan, L.; Li, L.; Mao, N.; Qin, X.; Peng, S.; Ramakrishna, S. Hierarchical catalytic electrodes of cobalt-embedded carbon nanotube/carbon flakes arrays for flexible solid-state zinc-air batteries. *Carbon* **2019**, *142*, 379–387. [[CrossRef](#)]
30. Jiang, G.; Jiang, N.; Zheng, N.; Chen, X.; Mao, J.; Ding, G.; Li, Y.; Sun, F.; Li, Y. MOF-derived porous Co_3O_4 -NC nanoflake arrays on carbon fiber cloth as stable hosts for dendrite-free Li metal anodes. *Energy Storage Mater.* **2019**, *23*, 181–189. [[CrossRef](#)]
31. Liang, Y.; Li, Y.; Wang, H.; Zhou, J.; Wang, J.; Regier, T.; Dai, H. Co_3O_4 nanocrystals on graphene as a synergistic catalyst for oxygen reduction reaction. *Nat. Mater.* **2011**, *10*, 780–786. [[CrossRef](#)] [[PubMed](#)]
32. Bai, B.; Arandiyani, H.; Li, J. Comparison of the performance for oxidation of formaldehyde on nano- Co_3O_4 , 2D- Co_3O_4 , and 3D- Co_3O_4 catalysts. *Appl. Catal. B Environ.* **2013**, *142*, 677–683. [[CrossRef](#)]
33. Chen, X.; Liu, B.; Zhong, C.; Liu, Z.; Liu, J.; Ma, L.; Deng, Y.; Han, X.; Wu, T.; Hu, W.; et al. Ultrathin Co_3O_4 layers with large contact area on carbon fibers as high-performance electrode for flexible zinc-air battery integrated with flexible display. *Adv. Energy Mater.* **2017**, *7*, 1700779. [[CrossRef](#)]

34. Zhang, Q.; Zhao, X.; Miao, X.; Yang, W.; Wang, C.; Pan, Q. ZIF-L-Co@carbon fiber paper composite derived Co/Co₃O₄@C electrocatalyst for ORR in alkali/acidic media and overall seawater splitting. *Int. J. Hydrogen Energy* **2020**, *45*, 33028–33036. [[CrossRef](#)]
35. Hu, Z.; Fu, Y.; Hong, Z.; Huang, Y.; Guo, W.; Yang, R.; Xu, J.; Zhou, L.; Yin, S. Composite structural batteries with Co₃O₄/CNT modified carbon fibers as anode: Computational insights on the interfacial behavior. *Compos. Sci. Technol.* **2021**, *201*, 108495. [[CrossRef](#)]
36. Sun, J.; Man, P.; Zhang, Q.; He, B.; Zhou, Z.; Li, C.; Wang, X.; Guo, J.; Zhao, J.; Xie, L.; et al. Hierarchically-structured Co₃O₄ nanowire arrays grown on carbon nanotube fibers as novel cathodes for high-performance wearable fiber-shaped asymmetric supercapacitors. *Appl. Surf. Sci.* **2018**, *447*, 795–801. [[CrossRef](#)]
37. Li, Y.; Zhong, C.; Liu, J.; Zeng, X.; Qu, S.; Han, X.; Deng, Y.; Hu, W.; Lu, J. Atomically thin mesoporous Co₃O₄ layers strongly coupled with N-rGO nanosheets as high-performance bifunctional catalysts for 1D knittable zinc-air batteries. *Adv. Mater.* **2018**, *30*, 1703657. [[CrossRef](#)] [[PubMed](#)]
38. Xi, Z.; Zhang, X.; Ma, Y.; Zhou, C.; Yang, J.; Wu, Y.; Li, X.; Luo, Y.; Chen, D. Recent progress in flexible fibrous batteries. *ChemElectroChem* **2018**, *5*, 3127–3137. [[CrossRef](#)]
39. Gao, Y.; Guo, Q.; Zhang, Q.; Cui, Y.; Zheng, Z. Fibrous materials for flexible Li-S battery. *Adv. Energy Mater.* **2021**, *11*, 2002580. [[CrossRef](#)]
40. Nan, D.; Huang, Z.-H.; Kang, F.-Y.; Shen, W.-C. Research progress on fibrous carbon materials as anode materials for lithium ion batteries. *Carbon* **2015**, *86*, 371. [[CrossRef](#)]
41. Deng, L.; Eichhorn, S.J.; Kao, C.-C.; Young, R.J. The effective Young's modulus of carbon nanotubes in composites. *ACS Appl. Mater. Interfaces* **2011**, *3*, 433–440. [[CrossRef](#)]
42. Wang, Y.; Jin, M.; Zhang, X.; Zhao, C.; Wang, H.; Li, S.; Liu, Z. Direct conversion of biomass into compact air electrode with atomically dispersed oxygen and nitrogen coordinated copper species for flexible zinc-air batteries. *ACS Appl. Energy Mater.* **2019**, *2*, 8659–8666. [[CrossRef](#)]
43. Zhang, X.; Liu, R.; Zang, Y.; Liu, G.; Liu, S.; Wang, G.; Zhang, Y.; Zhang, H.; Zhao, H. Shrimp-shell derived carbon nanodots as precursors to fabricate Fe,N-doped porous graphitic carbon electrocatalysts for efficient oxygen reduction in zinc-air batteries. *Inorg. Chem. Front.* **2016**, *3*, 910–918. [[CrossRef](#)]
44. Chang, S.; Hui, Z.; Zhang, Z. FeCo alloy/N, S dual-doped carbon composite as a high-performance bifunctional catalyst in an advanced rechargeable zinc-air battery. *J. Energy Chem.* **2021**, *56*, 64–71. [[CrossRef](#)]
45. Wang, X.; Liao, Z.; Fu, Y.; Neumann, C.; Turchanin, A.; Nam, G.; Feng, X. Confined growth of porous nitrogen-doped cobalt oxide nanoarrays as bifunctional oxygen electrocatalysts for rechargeable zinc-air batteries. *Energy Storage Mater.* **2020**, *26*, 157–164. [[CrossRef](#)]